Materials Transactions, Vol. 56, No. 11 (2015) pp. 1781 to 1786

Texture and Lattice Distortion Study of an Al-6061-T6 Alloy Produced by ECAP

Carlos Reyes-Ruiz[1,2], Ignacio A. Figueroa[1], Chedly Braham[2], José M. Cabrera[3,4], Ismeli Alfonso[5] and Gonzalo Gonzalez[1,2,*]

[1]*Instituto de Investigaciones en Materiales, Universidad Nacional Autónoma de México, Circuito exterior S/N, Cd. Universitaria, A.P. 70-360, Coyoacán, C.P. 04510, México*
[2]*Laboratoire Procédés et Ingénierie en Mécanique et Matériaux, UMR CNRS 8006, ENSAM, 151, bd de Hôpital 75013, Paris, France*
[3]*Departamento de Ciencia de los Materiales e Ingeniería Metalúrgica, ETSEIB-Universidad Politécnica de Cataluña, Av. Diagonal 647, 08028 Barcelona, Spain*
[4]*Fundación CTM Centro Tecnológico, Pl. de la Ciencia 2, 08243 Manresa, Spain*
[5]*Instituto de Investigaciones en Materiales, Unidad Morelia, Universidad Nacional Autónoma de México, Campus Morelia UNAM, Antigua Carretera a Pátzcuaro No. 8701, Col. Ex-Hacienda de San José de la Huerta, C.P. 58190 Morelia, Michoacán, México*

Equal channel angular pressing (ECAP) is a severe plastic deformation (SPD) technique that produces nanostructured materials. Based on a remarkable grain size reduction, this process has led to improve mechanical properties, such as yield strength, fatigue, UTS, etc. In this work the characterization of the microstructure of the aluminum 6061-T6 alloy; plastically deformed up to $\varepsilon \approx 6$, by the ECAP process, following route Bc, is presented. For this purpose, the ECAP processed samples were characterized by means of X-ray diffraction (for texture and line profile analysis) and transmission electron microscopy. The initial crystallographic texture vanished after one ECAP pass and a new, well defined, shear texture C_θ was generated. For the subsequent ECAP passes, more shear components: $A^*_{1\theta}$, B_θ and $\bar{B}_\theta$ were also developed. From the orientation distribution function analysis, a shift (generally less than 15°) between some experimental maxima and the reported ideal shear texture positions was observed. From these results, it was found that the microstructure generated with this process was stabilized after the 5th ECAP pass. Finally, the micro-strain analyses, in addition to the texture and transmission electron microscopy, contributed to the understanding of the effect of the physical and mechanical processes that were activated during the SPD-ECAP technique. [doi:10.2320/matertrans.M2015200]

(Received May 19, 2015; Accepted August 6, 2015; Published October 25, 2015)

Keywords: *aluminum alloys, equal channel angular pressing, crystal texture*

1. Introduction

It is well known that the severe plastic deformation processes (SPD) can produce structures with very fine grain size in bulk metallic alloys. Among these processes, equal channel angular pressing (ECAP) has been widely used due to its capacity to produce large strains whilst preserving the initial sample geometry. ECAP is a cumulative strain process that can increase the yield strength, fatigue life and toughness, among other important features.[1–3] A number of aluminum (Al) alloys have been tested by ECAP, but those which are age-hardenable tended to be more susceptible to the severe plastic deformation.[4] Within this context, the Al-6061 alloy has been analyzed under several conditions, i.e. different initial microstructural stages, peak aging, over-aging and solid solution. However, the highest ultimate tensile strength (UTS) value was found for the peak-aged alloys.[5,6]

Some detrimental features such as fragmentation of precipitates and recovery at room temperature have been related to peak-aged Al alloys.[6] As consequence, there is a reduced number of papers based, exclusively, on the Al-6061 alloy under a T6 treatment. On the other hand, for the Al-6061 alloy in the solid solution condition, processed by ECAP at 125°C, a couple of manuscripts have been reported.[6,7] The above mentioned manuscripts[5,6] reported an enhancement of ≈40% in UTS and yield stress (after a post-ECAP heat treatment), when compared to the commercial Al-6061-T6 (without ECAP deformation). Besides, Shokuhfar *et al.*[8] recently reported, the study of the Al-6061 alloy at O and T6 temper by ECAP within route C. The highest yield strength and the lowest ductility were found for the T6 temper sample.

It is well known that the crystal texture can strongly modify some physical properties of the final product, for instance: formability, work hardening, plastic anisotropy, fatigue life, etc. Although, the ECAP texture evolution has been already reported for 99.99% pure Al[9] and for a number of Al based alloys[2] as far as we know, there is no a single report in the literature that presents a detailed texture study for the Al-6061-T6 alloy processed by ECAP, at room temperature following route Bc, being the paper reported by Mckenzie and Lapovok the closest one.[10] On the other hand, it is important to mention that the study of the deformation (due to the dislocation array rearrangement) has an important scientific value for understanding the stabilization of the dislocation array. If such stabilization is found after a determined number of ECAP passes, it will not be necessary to continue the deformation process, i.e. adding more passes. From the above, the objective of this work was to study the texture evolution of an Al-6061-T6 alloy and the lattice distortion induced by the ECAP process at room temperature. The change in the misorientation of the crystallites as a function of the ECAP passes will also be assessed.

2. Experimental Procedure

Commercial Al-6061-T6 bars were cut at 60 mm in length and 10 mm in diameter, and were used as starting material (Table 1), no additional heat treatment was performed afterwards at the prepared alloy bars. The ECAP process was carried out at room temperature following route Bc (rotation along its longitudinal axis by 90° clockwise, before

*Corresponding author, E-mail: joseggr@unam.mx

Table 1 Nominal composition of the Al-6061 alloy.

Element	Si	Fe	Cu	Mn	Mg	Cr	Zn	Ti	Others	Al
% wt	0.4–0.8	0.7	0.15–0.4	0.15	0.8–1.2	0.04–0.35	0.25	0.15	0.05	balance

each extrusion). This route has been reported to be favorable for obtaining high microstructural homogenization with large misorientation angles.[11] The samples were extruded through a Böhler MICROCLEAN S390 steel die with two intersecting channels, having $\phi = 90°$ and $\psi = 37°$ as inner and outer angle, respectively (Fig. 1).

As ECAP produces cumulative strain, which increases as the number of passes rises, the samples were reintroduced up to 6 times into the ECAP die-set channel. According to the Iwahashi's equation,[12] this leads to a maximum equivalent strain $\varepsilon \approx 6$. During the ECAP deformation process, the average strain rate calculated was $\dot{\varepsilon} \approx 0.3\,s^{-1}$, and MoS_2 spray compound was used as lubricant for reducing the friction between the sample and the steel die. The samples were cut in different cross sections, depending on the characterization technique. Vickers microhardness tests were performed on every highly deformed sample, using a Vickers diamond indenter. The microhardness tester used in this work was a Matsuzawa model MMT-X7A. The software of the equipment takes the measured indentation and converts it to a hardness value. The microhardness testing in this work was carried out using a load of 100 g with a holding time of 10 s. Each test value was taken from an average of ten indentations, with an experimental error lower than ±10%.

Transmission electron microscopy (TEM) observations were carried out on a 120 kV microscope (JEOL 120EX), selection area diffraction (SAD) patterns were taken over regions having a 5 μm in diameter, and thin foils were obtained by means of focus ion beam thinning (JEM-9320FIB) on plane TD (see Fig. 1).

For the texture measurements, samples were mechanically grinded and electro-polished till obtaining a mirror-like appearance. The analysis was carried out with a RIGAKU-ULTIMA IV X-ray diffractometer, equipped with crossbeam optics (CBO), wavelength Cu-Kα (0.15405 nm). The measurements were made in mode "in plane", with a ranging scan α and β of 0–90° and 0–360°, respectively. 3D EXPLORE software was used as visualizing tool. The orientation distribution functions (ODF) plots were calculated by means of MTEX (MatLab tool box).[13]

The X-ray peak-broadening was calculated based on the Rietveld refinement method. The data were collected from 20 to 140° in 2θ range, with a step size of 0.02°. The analyzed section was the normal plane (NP), as shown in Fig. 1. The measurements were carried out by keeping the same direction, ED, for all samples. The instrumental peak width was calculated using a LaB_6 standard powder. FULLPROF software[14] was used for deconvoluting the sample half maximum (FWHM) and integral breadth from its Gaussian and Lorentzian contribution. Further details of this specific calculation can be found in reference.[15]

Assuming a Lorentzian profile, the Willianson-Hall (W-H) equation permits to split the strain (ε) and crystallite domain size (D) contribution from the integral breadth (β), as follows:

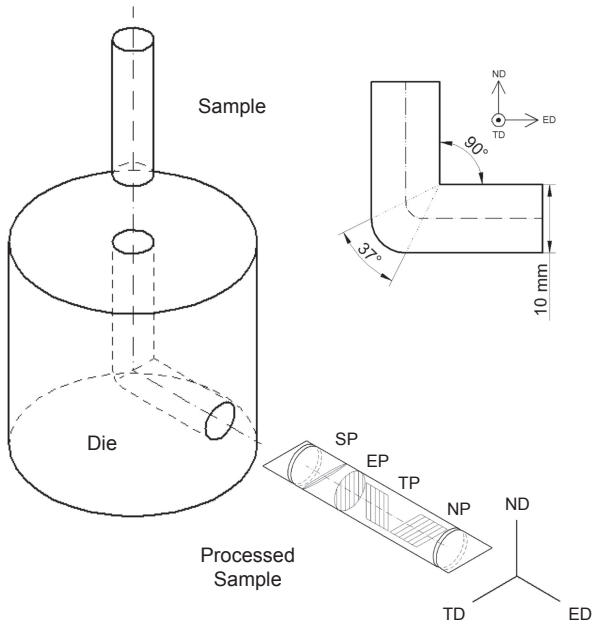

Fig. 1 Experimental setup and reference axis. ED, ND and TD are the extrusion, normal and transversal directions, and NP, TP, EP and SP are the normal, transversal, extrusion and shear planes, respectively.

$$\beta\cos(\theta) = \frac{\lambda}{D} + 4\varepsilon(\sin(\theta)) \tag{1}$$

The crystallite domain size and the strain can be acquired by plotting $\beta\cos(\theta)$ vs $\sin(\theta)$. From this plot, the y-intercept and the slope from a linear fitting can be obtained. It is worth mentioning that, when the values of the slope are different from zero, there is some strain contribution to the peak broadening. On the other hand, when the crystallites size is lower than 100 nm in diameter, the determination of such size is highly accurate. The Williamson-Hall plots provide valuable-qualitative information in order to visualize the variation of the strain as a function of ECAP passes.

3. Results and Discussions

From the evolution of the microhardness with the ECAP passes (Fig. 2), a possible asymptote at the end of the microhardness curve can be observed. This indicates that the microhardness, marginally, increased at ECAP passes ≥5. The X-ray diffraction patterns measured at the NP plane showed, qualitatively, the initial texture and its evolution as a function of the ECAP passes (Fig. 3). As expected, a notably change occurred after the first pass, in which the initial texture was severely modified. This must be balanced up with the fact that there is a relatively poor experimental statistic, as the initial grain size of the sample was rather large, i.e. between 200 and 300 μm. It is worth noting that, from the first ECAP pass, a continuous but not abrupt modification of intensities ratio did occur.

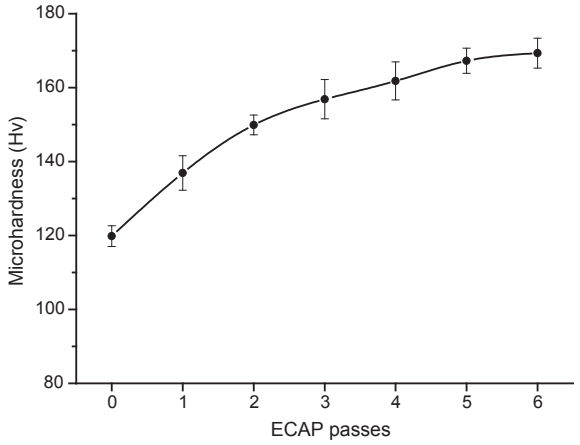

Fig. 2 Microhardness evolution as a function of the ECAP passes.

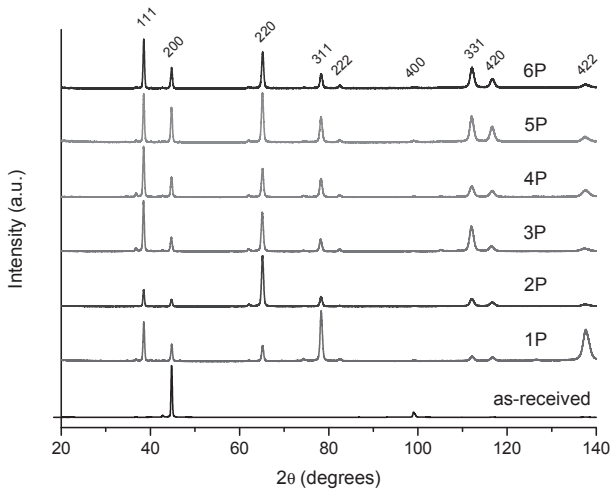

Fig. 3 X-ray diffractograms corresponding to all ECAP passes.

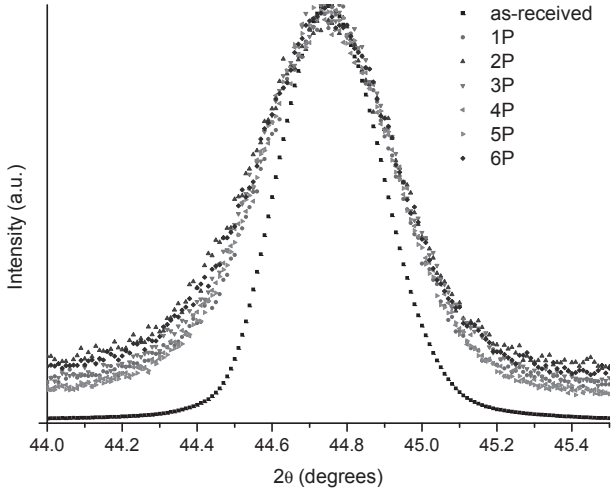

Fig. 4 X-ray peak broadening for plane (200) as a function of the ECAP passes.

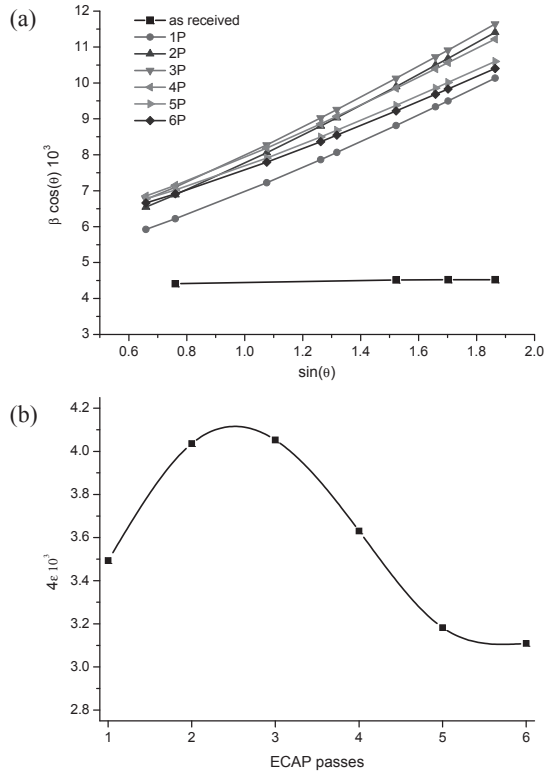

Fig. 5 (a) Williamson-Hall plots for different ECAP passes (N). (b) Slope variation ($\sim 4\varepsilon$) as a function of ECAP passes.

As an example, Fig. 4 graphically shows the width evolution for plane (200) as a function of ECAP passes. From this, it can be seen that the peak width drastically increased between 0 and 1 pass, reaching a maximum after the second pass, and then, the peak width decreased progressively. Rietveld refinement was used with the aim of evaluating, quantitatively, this behavior. From this refinement, the lattice parameters were found to be independent of the ECAP passes, the obtained lattice parameter value ($a = 0.4050$ nm) was compatible with the lattice parameter for the Al-6061 alloy at the peak age condition. The diffraction peak broadening is related with the micro-strain in the sample; such correlation is better illustrated by the characteristic Williamson-Hall plots (Fig. 5).

The magnitude of the slope from the Williamson-Hall plots showed that the strain dramatically increased between the as-received sample condition and the first ECAP pass. At two ECAP passes a maximum strain was found, then, this decreased down forming a plateau after the fifth ECAP pass, confirming the qualitative analysis previously described and shown in Fig. 4.

The crystallite size decreased as a function of ECAP passes, having a ratio of 1 : 0.77, between the first and sixth pass. The reduction in the crystallite size multiplied the grain boundaries that work as dislocation sinks, reducing the pile-up at grain boundaries. Hence, even though the dislocation sources are activated during the deformation, the density of dislocations did not grow at the same ratio. Notwithstanding the fact that the plastic deformation mechanism in nanocrystalline alloys is still controversial,[16–18] this behavior can be attributed to the dynamic recovery generated by the competition between dislocation multiplication and annihilation. This dynamic recovery could explain the strain reduction and stabilization between 4 and 6 ECAP passes, suggesting that the optimum number of ECAP passes for obtaining the most stable configuration, at least for the studied alloy, has been reached. Thus, the texture will remain

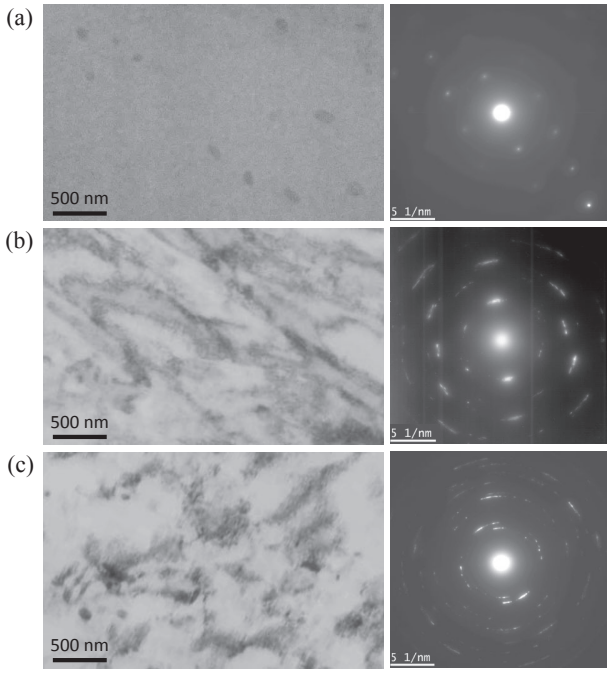

Fig. 6 TEM images and SAD patterns of (a) as-received sample, (b) after 1 ECAP pass, (c) after 6 ECAP passes.

constant and, therefore, the necessity of increasing the plastic deformation will not be necessary, i.e. adding more ECAP passes to the process. This assumption will be further discussed below, when comparing poles figures with some results reported in the literature.

The transmission electron images and their corresponding diffraction patterns are shown in Fig. 6. These images showed the transit between a single grain contrast, appearing with some precipitates Fig. 6(a), to a characteristic subgrain bands Figs. 6(b) and 6(c). Besides, the formation of incomplete diffraction rings in the SAD patterns, which tended to be more continuous as the number the ECAP passes increased, were rather compatible with the reduction of such grain size.

Figure 7 shows, in parallel view with respect to TD, the crystallite preferential orientation studied by means of pole figure representations. It is important to mention that, immediately after the first pass, the initial texture was highly modified by the ECAP process and the pole figures were easily interpreted for the first, second and third ECAP passes. This was attributed to the fact that they have just one or two texture components. However, after the fourth pass, several overlapped components appeared, therefore, the use of the ODF was highly necessary for their interpretation. It can be observed that the absolute texture intensity decreased with the number of ECAP passes (between the first and last pass) in a 12 : 1 ratio, according to ODF intensities. This can be explained by the formation of new grains with random orientations. On the other hand, the texture shown in Fig. 7(g) displays a clear similarity with those reported by El-Danaf *et al.*,[19] which have been labeled as a stable texture for the Bc route. The results from the aforementioned texture stabilization and W-H slopes could tell us that the deformation process has, probably, reached the number of optimal ECAP passes. Therefore, the W-H analysis seems to

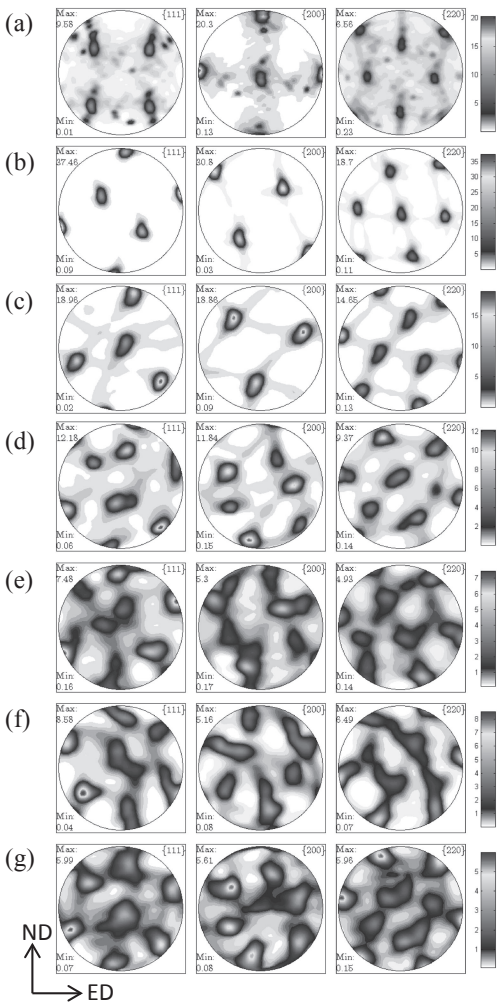

Fig. 7 Pole figures for the samples processed by ECAP after (a) 0, (b) 1, (c) 2, (d) 3, (e) 4, (f) 5, and (g) 6 passes using route Bc.

be an easy way to get this threshold for, at least, this alloy system.

With the aim of completing the texture study, the ODFs were calculated from the (111), (200), (220) pole figures. Figure 8 shows the different ODFs taken from all ECAP passes. Table 2 resumes the shear texture components obtained in this study.[20] The starting material, before the ECAP process, showed a cube texture (Fig. 8(a)). For the first ECAP pass, Fig. 8(b), the initial texture evolved for the original cube texture to C_θ, being tilted less than 5° from their ideal position. After two ECAP passes, the maximum orientation density was slightly shifted (less than 3°) away from the B_θ component, as shown in Fig. 8(c). Figure 8(d) shows the sample subjected to three ECAP passes, here, $A^*_{1\theta}$ was the main texture component observed. In the processing condition, corresponding to four ECAP passes (Fig. 8(e)) three main components were found, $A^*_{1\theta}$, B_θ and $\bar{B}_\theta$, being found at 3°, 15° and 12°, shifted away from the ideal positions, respectively. For five ECAP passes (Fig. 8(f)), the $A^*_{1\theta}$ component started to vanish away, the component, B_θ, was tilted away 21°, and $\bar{B}_\theta$ was found at 25°. Finally, after six ECAP passes, Fig. 8(g), only the components B_θ and $\bar{B}_\theta$ were identified, these components were shifted away (less than 6°) from the ideal positions.

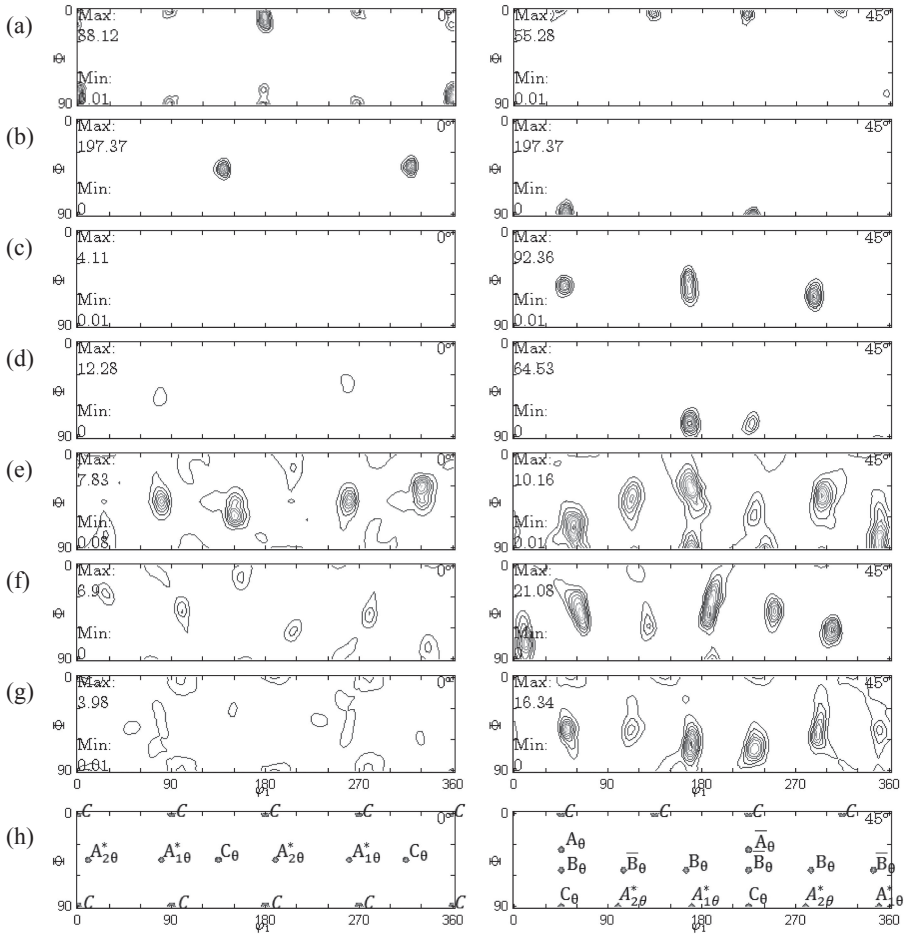

Fig. 8 ODF texture sections measured after (a) 0, (b) 1, (c) 2, (d) 3, (e) 4, (f) 5, (g) 6 ECAP passes, and (h) key positions for $\varphi_2 = 0°$ and 45°.

Table 2 ECAP shear textures for FCC materials.[20)]

Notation	Euler angles (°)[a]			Miller indices			Fibers it belongs to
	φ_1	Φ	φ_2	ND (approximate)	ND (approximate)	TD	
$A^*_{1\theta}$	80.26/260.26	45	0	[8 1 $\bar{1}$]	[1 $\bar{4}$ 4]	[0 1 1]	$\{1\ 1\ 1\}_\theta$
	170.26/350.26	90	45				
$A^*_{2\theta}$	9.74/189.74	45	0	[1 $\bar{4}$ 4]	[8 1 $\bar{1}$]	[0 1 1]	$\{1\ 1\ 1\}_\theta$
	99.74/279.74	90	45				
A_θ	45	35.26	45	[9 1 4]	[1 11 $\bar{5}$]	[$\bar{1}$ 1 2]	$\{1\ 1\ 1\}_\theta, \langle 1\ 1\ 0\rangle_\theta$
$\bar{A}_\theta$	225	35.26	45	[$\bar{1}$ $\bar{11}$ 5]	[$\bar{9}$ $\bar{1}$ $\bar{4}$]	[$\bar{1}$ 1 2]	$\{1\ 1\ 1\}_\theta, \langle 1\ 1\ 0\rangle_\theta$
B_θ	45/165/285	54.74	45	[15 4 11]	[7 26 $\overline{19}$]	[$\bar{1}$ 1 1]	$\langle 1\ 1\ 0\rangle_\theta$
$\bar{B}_\theta$	105/225/345	54.74	45	[$\bar{7}$ $\overline{26}$ 19]	[$\overline{15}$ $\bar{4}$ $\overline{11}$]	[$\bar{1}$ 1 1]	$\langle 1\ 1\ 0\rangle_\theta$
C_θ	135/315	45	0	[3 3 4]	[2 2 $\bar{3}$]	[$\bar{1}$ 1 0]	$\langle 1\ 1\ 0\rangle_\theta$
	45/225	90	45				

[a]Given in the $\varphi_2 = 0°$ and 45° sections only.

It is worth mentioning that most experimentally obtained texture components fitted well with the ideal positions, i.e. between 5 and 15°. Furthermore, the texture evolution corresponded, initially, to that predicted by the shear model reported in Refs. 19, 21). As it has already been published,[21)] the ODFs produced by the ECAP process appeared slightly tilted when compared to that of the ideal position for the texture shear components. Such shift is more pronounced within the four and five ECAP passes. The physical meaning of such tilts from the expected values, has been attributed to friction effects and die geometry.[21)]

4. Conclusions

The Al-6061-T6 alloy was successfully ECAPed at room temperature, the precipitates (at T6 condition) did not inhibit the angular extrusion of the samples. The electron diffraction patterns were compatible with a decrease in the strength of

preferred orientation between crystallites, especially at higher number of ECAP passes. The drop in the texture intensity indicates that the ECAP process generates an initial texture, which progressively decreases in a ratio of 12 : 1 between the first and sixth passes. Therefore, the ECAP process involves both disorientation and multiplication of crystallites boundaries.

According to the X-ray analysis for peak broadening, the micro-strain varies with the number of passes, having a maximum between 2 and 3 passes, then remains steady between 5 and 6 passes. This can be interpreted as the optimum number of ECAP passes in order to achieve a stable configuration of dislocations. The Al-6061-T6 initial texture disappeared in the first ECAP pass and the formation of a new characteristic ECAP shear texture was formed. Tilts generally less than 15° were observed between the ideal and measured texture components, this could be attributed to friction geometric effects. The reasonably good match between the texture results and W-H allows to speculate that the existence of the "plateau" and the texture stability are related. Finally, the W-H analysis could be used as a rather useful tool to find out the number of optimal ECAP passes, being also applicable to other methods for severe plastic deformation.

Acknowledgments

G. Gonzalez would like to thank the financial support from CONACYT and PAPIIT through projects No. 166896 and IN110014. This research was carried out during the sabbatical year of GG at ENSAM-CNAM with the support of PASPA-UNAM and CONACYT.

REFERENCES

1) R. Z. Valiev and T. G. Langdon: Prog. Mater. Sci. **51** (2006) 881–981.
2) I. Sabirov, M. Yu. Murashkin and R. Z. Valiev: Mater. Sci. Eng. A **560** (2013) 1–24.
3) Z. Horita, T. Fujinami, M. Nemoto and T. G. Langdon: J. Matter. Proc. Technol. **117** (2001) 288–292.
4) H. J. Roven, H Nesboe, J. C. Werenskiold and T. Seibert: Mater. Sci. Eng. A **410–411** (2005) 426–429.
5) S. Ferrasse, V. M. Segal, K. T. Hartwig and R. E. Goforth: J. Mater. Res. **12** (1997) 1253–1261.
6) J. K. Kim, H. G. Jeong, S. I. Hong, Y. S. Kim and W. J. Kim: Scr. Mater. **45** (2001) 901–907.
7) C. S. Chung, J. K. Kim, H. K. Kim and W. J. Kim: Mater. Sci. Eng. A **337** (2002) 39–44.
8) A. Shokuhfar and O. Nejadseyfi: Mater. Sci. Eng. A **594** (2014) 140–148.
9) S. D. Terhune, D. L. Swisher, K. OH-Ishi, Z. Horita, T. G. Langdon and T. R. McNelley: Metall. Mater. Trans. A **33** (2002) 2173–2184.
10) P. W. J. Mckenzie and R. Lapovok: Acta Mater. **58** (2010) 3198–3211.
11) Y. Iwahashi, Z. Horita, M. Nemoto and T. G. Langdon: Acta Mater. **46** (1998) 3317–3331.
12) Y. Iwahashi, J. Wang, Z. Horita, M. Nemoto and T. G. Langdon: Scr. Mater. **35** (1996) 143–146.
13) F. Bachmann, R. Hielscher and H. Schaeben: Solid State Phenomena **160** (2010) 63–68.
14) T. Roisnel and J. Rodriguez-Carbajal: Mater. Sci. Forum **378–381** (2001) 118–123.
15) G. Gonzalez, C. Braham, J. L. Lebrun, Y. Chastel, W. Seiler and I. Figueroa: Mater. Trans. **53** (2012) 1234–1239.
16) M. A. Meyers, A. Mishra and D. J. Benson: Prog. Mater. Sci. **51** (2006) 427–556.
17) W. Skrotzki, A. Eschke, B. Jóni, T. Ungár, L. S. Tóth, Yu. Ivanisenko and L. Kurmanaeva: Acta Mater. **61** (2013) 7271–7284.
18) A. A. Tohidi, M. Ketabchi and A. Hasannia: Mater. Sci. Eng. A **577** (2013) 43–47.
19) E. A. El-Danaf: Mater. Sci. Eng. A **492** (2008) 141–152.
20) S. Li, I. J. Beyerlein and M. A. M. Bourke: Mater. Sci. Eng. A. **394** (2005) 66–77.
21) I. J. Beyerlein and L. S. Tóth: Prog. Mater. Sci. **54** (2009) 427–510.